ACS APPLIED MATERIALS & INTERFACES

www.acsami.org

Research Article

Effect of Additives on the Surface Morphology, Energetics, and Contact Resistance of PEDOT:PSS

Alexander X. Chen, Guillermo L. Esparza, Ignasi Simon, Sean P. Dunfield, Yi Qie, Jordan A. Bunch, Rachel Blau, Allison Lim, Henry Zhang, Sarah E. Brew, Finnian M. O'Neill, David P. Fenning,* and Darren J. Lipomi*

Cite This: *ACS Appl. Mater. Interfaces* 2023, 15, 38143–38153

Read Online

ACCESS | Metrics & More | Article Recommendations | Supporting Information

ABSTRACT: For a poly(3,4-ethylenedioxythiophene) polystyrene sulfonate (PEDOT:PSS) film employed in a device stack, charge must pass through both the bulk of the film and interfaces between adjacent layers. Thus, charge transport is governed by both bulk and contact resistances. However, for ultrathin films (e.g., flexible devices, thin-film transistors, printed electronics, solar cells), interfacial properties can dominate over the bulk properties, making contact resistance a significant determinant of device performance. For most device applications, the bulk conductivity of PEDOT:PSS is typically improved by blending additives into the solid film. Doping PEDOT:PSS with secondary dopants (e.g., polar small molecules), in particular, increases the bulk conductivity by inducing a more favorable solid morphology. However, the effects of these morphological changes on the contact resistance (which play a bigger role at smaller length scales) are relatively unstudied. In this work, we use transfer length method (TLM) measurements to decouple the bulk resistance from the contact resistance of PEDOT:PSS films incorporating several common additives. These additives include secondary dopants, a silane crosslinker (typically used to stabilize the PEDOT:PSS film), and multi-walled carbon nanotubes (conductive fillers). Using conductive atomic force microscopy, Kelvin probe force microscopy, Raman spectroscopy, and photoelectron spectroscopy, we connect changes in the contact resistance to changes in the surface morphology and energetics as governed by the blended additives. We find that the contact resistance at the PEDOT:PSS/silver interface can be reduced by (1) increasing the ratio of PEDOT to PSS chains, (2) decreasing the work function, (3) decreasing the benzoid-to-quinoid ratio at the surface of the solid film, (4) increasing the film uniformity and contact area, and (5) increasing the phase-segregated morphology of the solid film.

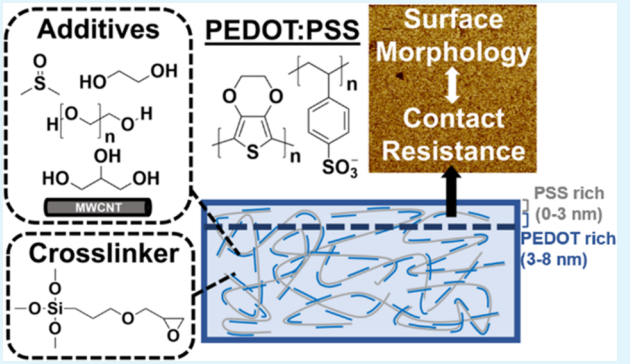

KEYWORDS: *semiconducting polymers, PEDOT:PSS, contact resistance, surface characterization, energetics, transfer length method, thin-film morphology, additives*

INTRODUCTION

The conductive polyelectrolyte complex PEDOT:PSS is used ubiquitously in organic optoelectronic and bioelectronic devices. In these applications, charge transfer from electronic materials, skin, and internal organs is mediated by the surface of the electrode, active layer, or sensing layer. Despite extensive investigation into the bulk electronic properties[1−7] of solid PEDOT:PSS films, comparatively few studies have investigated the electronic properties of the surface, and in particular, the ways in which they affect the contact resistance. At an interface between materials, the composition and morphology determine the ease at which charge can travel from one surface to another.[8,9] Thus, decreasing the contact resistance of an interface offers a way to increase the overall current that can travel through a device stack, particularly for applications employing ultrathin films (e.g., organic field effect transistors[10,11] or solar cells).

The contact resistance between two surfaces is dependent on several factors. First, on physical contact (i.e., contact area[12] and contact mechanics), as dependent on, e.g., topography and roughness.[13] Second, the contact resistance is dependent on the Schottky barrier between the two materials, which is governed by their energetics (e.g., alignment of the metal work function with the valence and conduction bands of the semiconductor) and the existence of a trapped density of states at the interface.[10] Third, transport across two surfaces in

Received: June 9, 2023
Accepted: July 17, 2023
Published: July 27, 2023

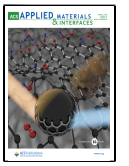

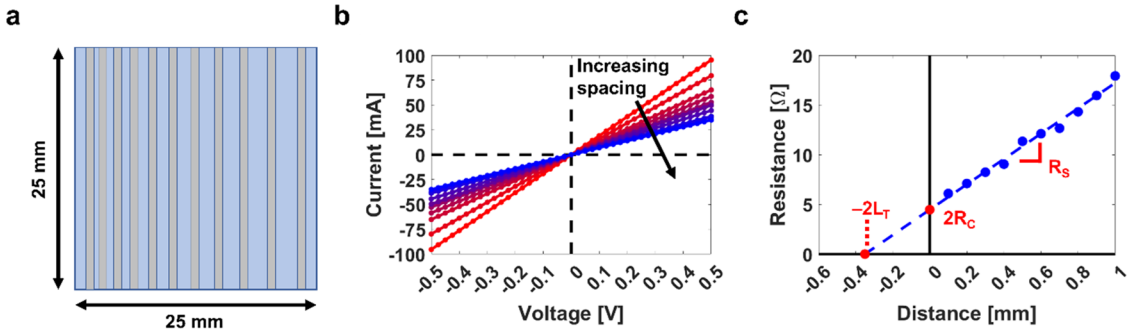

Figure 1. (a) Schematic of evaporated transfer length method (TLM) contacts (silver, 1.6 mm × 25 mm) on a PEDOT:PSS film. Eleven contacts were evaporated to measure 10 different spacings (0.1−1 mm, in increments of 0.1 mm). (b) Current−voltage (I−V) measurements were conducted at each of the 10 different spacings. (c) Resistance was calculated from Ohm's law and plotted relative to spacing. The data was fit using a linear regression, from which the sheet resistance (R_S), contact resistance (R_C), and transfer length (L_T) could be extracted. Using the geometry of the metal contacts and film thickness, the bulk resistivity (ρ) and contact resistivity (ρ_C) were calculated.

contact can be hindered by charge trapping mechanisms[14,15] at the interface. Trapped charges can arise due to morphology,[16,17] molecular composition, or the formation of a new (usually unintended) interfacial layer, e.g., from the presence of oxides, water, or volatile organic compounds.[13]

Thus, the contact resistance of PEDOT:PSS should be dependent on the surface morphology of the solid film, which can be manipulated by changing the composition in solution and the process of solidification. Several investigations suggest that the inclusion of secondary dopants can result in the removal of nonconductive PSS chains at the surface of the film. For example, work by Jönsson et al. has shown that blending sorbitol and *N*-methylpyrrolidone into PEDOT:PSS results in a solid film with a decreased ratio of PSS to PEDOT at the surface, as measured using X-ray photoelectron spectroscopy (XPS).[2] Crispin et al. observed a similar effect, in which the addition of ethylene glycol (EG) reduced the thickness of insulating PSS layers surrounding conductive PEDOT domains.[18] Additionally, post-deposition treatments, such as dipping a PEDOT:PSS film in an aqueous solution of dimethyl sulfoxide (DMSO)[19] or gentle application of EG or DMSO to the film surface,[12] have been shown to achieve similar morphological changes that are likely to result in differences in contact resistance.

In contrast, strategies for increasing the bulk conductivity of PEDOT:PSS films have been well explored. The most common is the incorporation (e.g., blending) of polar small molecules as secondary dopants (e.g., EG, DMSO) in solution.[2−5,20] For example, the addition of DMSO in PEDOT:PSS (Clevios PH1000) has been used to achieve conductivities greater than 600 S cm^{-1}.[3,21−23] When coupled with post-deposition treatments (e.g., an H_2SO_4 treatment), such PEDOT:PSS films have achieved conductivities of >4000 S cm^{-1}.[24] A number of reviews[1−6,25] and research papers[20,26−36] discuss in detail the mechanisms by which the increase of the electrical (and ionic) conductivity of PEDOT:PSS is achieved. In general, enhancements in conductivity are attributed to changes in the morphology of the solid film, which consists typically of bundled grains composed of a PEDOT-rich core and surrounded by PSS.[28] Evidence suggests that the addition of secondary dopants results in the formation of larger PEDOT domains coupled with greater phase segregation, resulting in reduced insulation between PEDOT-rich domains,[4] stronger π−π coupling for charge transport and an improved crystalline morphology,[32] as well as a more favorable three-dimensional conduction pathway.[20,28] A second strategy has been to incorporate conductive materials, such as carbon nanotubes, as an electronic filler. While carbon nanotubes are highly conductive, only low loadings are typically able to be dispersed in a PEDOT:PSS solution without affecting the quality of the film. For example, Hegde et al. reported that PEDOT:PSS films dispersed with 0.1 wt % of multi-walled carbon nanotubes (MWCNT) achieved conductivities of 0.14 S cm^{-1}.[37] Additional studies suggest that the electrical conductivity of PEDOT:PSS/CNT films correlates directly with an increase in CNT loading.[38−40] Some studies[41,42] have simultaneously employed both additive strategies by incorporating both secondary dopants and CNT in PEDOT:PSS films, reaching a maximum conductivity of >2600 S cm^{-1}.[41] Finally, other studies have described how synthetic modifications can be performed on PEDOT:PSS in order to increase their stability, mechanical conformability, and reliability for potential device applications.[26,27] For example, the PEDOT:PSS film can be crosslinked[43,44] to increase the mechanical stability of PEDOT:PSS (particularly for applications with biological interfaces,[45,46] e.g., organic electrochemical transistors[47−49]). However, crosslinking PEDOT:PSS (e.g., with (3-glycidyloxypropyl)trimethoxysilane, GOPS) decreases the bulk conductivity of the solid film.[43] Thus, ensuring favorable electronic properties of a crosslinked PEDOT:PSS film also requires inclusion of a secondary dopant.

Studies that report contact resistivity and/or contact resistance generally use the transfer length method (TLM), a modified version of the transmission line measurement.[8,50] For example, Pretl et al. reported contact resistances of dip-coated PEDOT:PSS films with gold electrodes to be dependent on the ratio of PEDOT to PSS.[51] Additionally, for a common commercial formulation of PEDOT:PSS (Clevios PH1000), Hoppe et al. found the contact resistivity of films with aluminum contacts to be 0.2 Ω cm^2.[52] When blended with 5 vol % DMSO and 0.1 vol % Capstone FS-31, Mahato et al. measured the contact resistivity with silver contacts to be 0.8 Ω cm^2.[53] In comparison, Kirihara et al. measured the contact resistivity between PEDOT:PSS and a silver−copper composite to be 1.1 Ω cm^2.[12] Additionally, these authors showed that drop-cast films of PEDOT:PSS, when blended with ethylene glycol (EG), dimethyl sulfoxide (DMSO), or poly(ethylene glycol) (PEG), achieved contact resistivities between 0.022 and 0.028 Ω cm^2 with contacts deposited using silver paste (a

https://doi.org/10.1021/acsami.3c08341
ACS Appl. Mater. Interfaces 2023, 15, 38143−38153

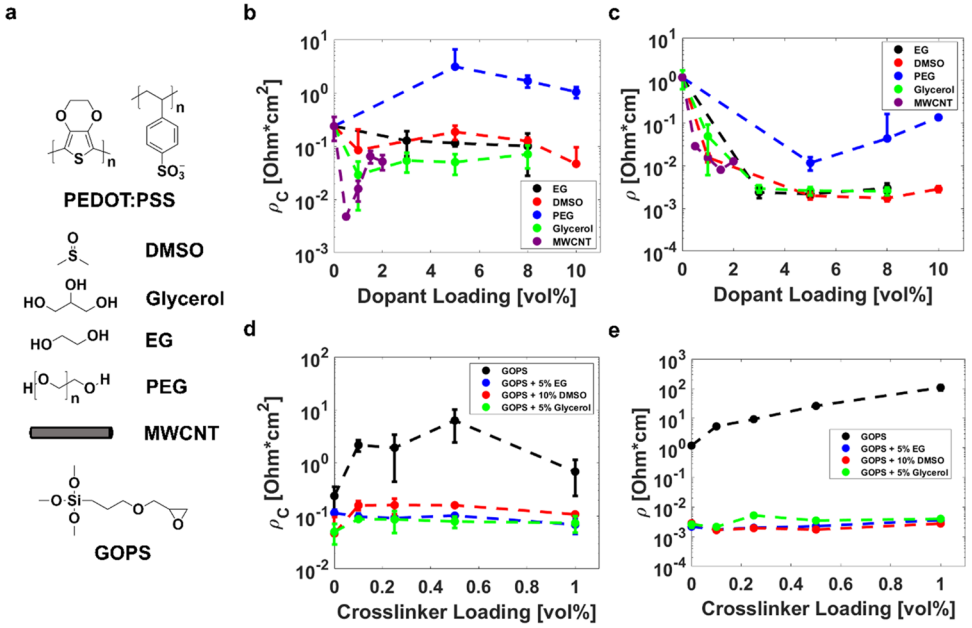

Figure 2. Contact and bulk electronic properties of PEDOT:PSS. (a) Chemical structures of dopants (dimethyl sulfoxide (DMSO), glycerol, ethylene glycol (EG), and poly(ethylene glycol) (PEG)) and of the crosslinker (3-glycidyloxypropyl)trimethoxysilane (GOPS). (b) Contact resistivity and (c) bulk resistivity relative to additive loading determined from TLM. The effect of crosslinker loading, as well as crosslinker incorporated with EG, DMSO, and glycerol as secondary dopants, on the (d) contact resistivity and (e) bulk resistivity of PEDOT:PSS determined using TLM.

silver−copper composite).[12] To further decrease (i.e., improve) the contact resistivity to 0.011−0.022 Ω cm^2, a post-deposition surface treatment (using DMSO or EG) was used to create a wavy surface topography, hence increasing the contact area at the PEDOT:PSS/silver−copper interface. However, connecting changes in film morphology induced by secondary doping effects to changes in the contact properties has remained unexplored.

In this work, we use the TLM method to investigate how the incorporation of secondary dopants, GOPS, and MWCNT affect the contact resistivity of PEDOT:PSS (Clevios PH1000) (Figure 1), as explained by changes in the surface morphology of the solid film. We connect these measurements to the characterization of these PEDOT:PSS films using conductive atomic force microscopy (c-AFM), Kelvin probe force microscopy (KPFM), Raman spectroscopy, X-ray photoelectron spectroscopy (XPS), and ultraviolet photoelectron spectroscopy (UPS).

EXPERIMENTAL DESIGN

Selection of Materials. A commercially available formulation of PEDOT:PSS (Clevios PH1000, Heraeus), as well as four different dopants (ethylene glycol, poly(ethylene glycol), dimethyl sulfoxide, and glycerol) were chosen for this study because they are widely studied in the literature and easily accessible from commercial vendors. We chose to study blended films (as opposed to films also exposed to post-deposition treatments) because doped PEDOT:PSS films are commonly used for device applications. We also included multi-walled carbon nanotubes (MWCNTs) as an additive because they are commonly used as a conductive filler. The average outer diameter of all MWCNTs used was 8 nm unless otherwise stated. We chose to study how crosslinking the PEDOT:PSS film with GOPS affects contact resistance because GOPS is commonly used to stabilize PEDOT:PSS for implantable bioelectronics.[47,54] We selected silver for the metal contacts because many optoelectronic applications (e.g., solar cells) use silver electrodes, although most bioelectronic applications use gold or platinum.

Measurement of Electronic Properties. To measure the bulk and contact resistance of PEDOT:PSS thin films (which we convert using the geometry of the sample to bulk and contact resistivity), we used the transfer length method (TLM), a modified form of the transmission line measurement.[8,50] Here, the transfer length represents the characteristic decay in charge transfer at the semiconductor/metal interface, which drops off exponentially from the leading edge of the metal pad. A custom evaporation shadow mask was designed to have 11 contacts (thus 10 measurements per sample). We repeated these measurements for at least three samples per condition to calculate the standard deviation. In some cases, TLM measurements resulted in clear outliers within a film (i.e., relative to the linear regression from the rest of the data). These outliers typically occurred at the 0.1 or 1 mm measurements due to nonuniform regions of the film at the edges of the substrates. These data points were removed during data processing, but all linear regressions used to calculate the sheet resistance (the slope of the linear regression) and the contact resistance (the y-intercept) had at least 7 data points (i.e., measurements at different spacings) with a coefficient of determination (R^2) greater than 0.9.

Characterization of Surface Morphology, Composition, and Energetics. Conductive AFM (c-AFM) was performed to characterize the surface conductance of representative PEDOT:PSS films. The bias, scan rate, pre-gain correction, and post-gain correction used were constant for all samples to prevent any parameter-dependent differences in the AFM scans. We collect the height and current plots concurrently. Because the contact resistance is also dependent on the work functions of the two materials in contact, we elect to perform Kelvin probe force microscopy (KPFM) measurements to characterize the work function of the PEDOT:PSS film. We compare these work function measurements to those collected by ultraviolet photoelectron spectroscopy (UPS). To qualitatively compare the ratio of quinoid to benzoid species, we use Raman spectroscopy. To elucidate the proportion of PEDOT to PSS at the surface of the film, we use X-ray photoelectron spectroscopy (XPS). Detailed methodologies are included in the Supporting Information.[55,56]

https://doi.org/10.1021/acsami.3c08341
ACS Appl. Mater. Interfaces 2023, 15, 38143−38153

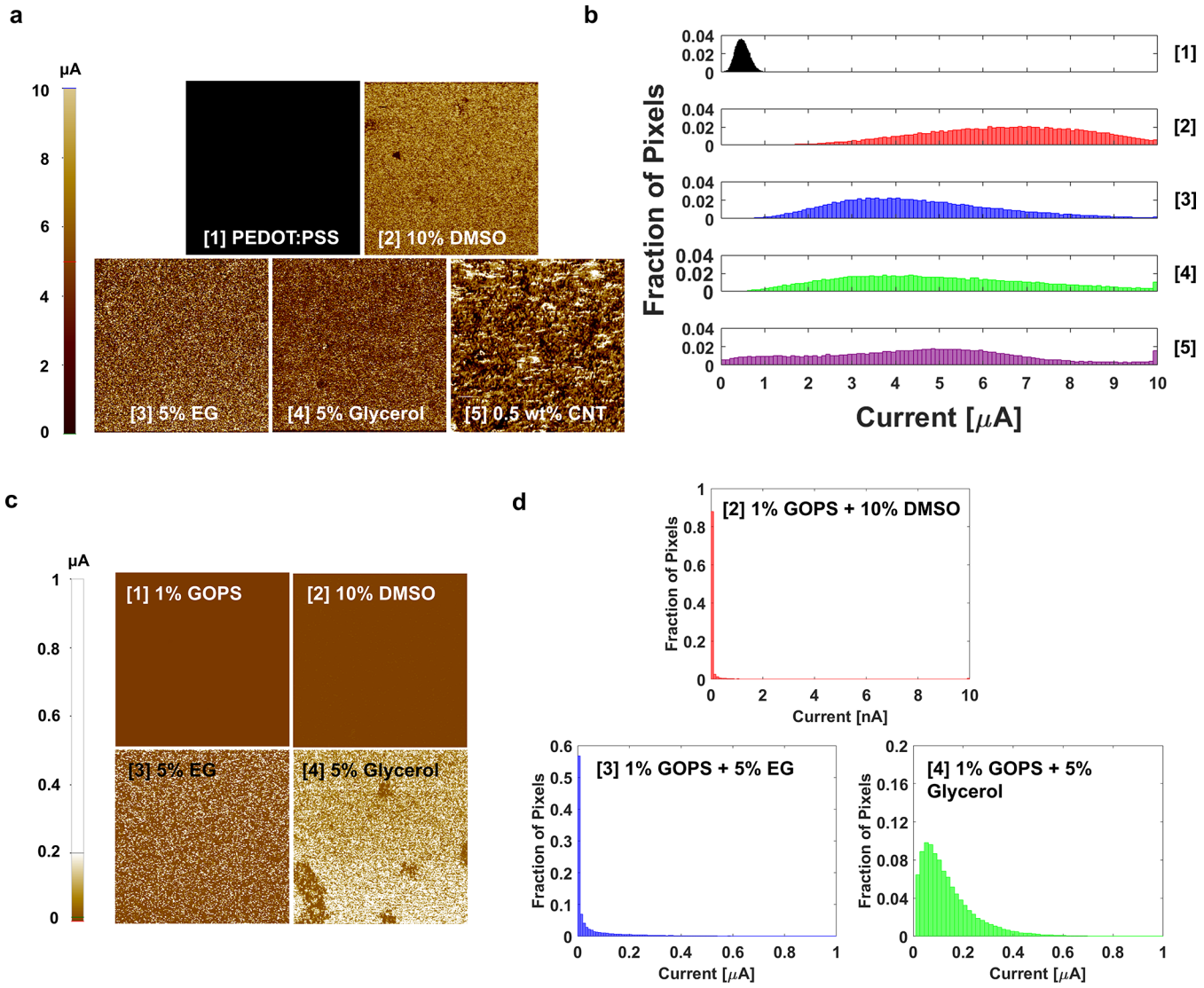

Figure 3. Conductive AFM measurements of PEDOT:PSS films. (a) Current plots for pristine PEDOT:PSS and PEDOT:PSS blended with DMSO, EG, glycerol, and MWCNT. (b) Histograms comparing the distribution of measured currents over the measured 5 μm × 5 μm surface of each film. (c) Current plots of PEDOT:PSS films crosslinked with GOPS (1%) and blended with different secondary dopants (DMSO, EG, glycerol). (d) Histograms for the crosslinked films (1% GOPS) blended with secondary dopants.

RESULTS AND DISCUSSION

We compare the bulk and contact resistivity, as measured by TLM, for PEDOT:PSS films blended with each additive (Figure 2a), as shown in Figure 2b–e.

Previous reports suggest that the contact resistivity for different compositions of PEDOT:PSS (and often to different metal contacts) varies between 0.2 and 1.1 Ω cm^2,[12,52,53] a relatively wide distribution. Here, we measured the contact resistivity of pristine PEDOT:PSS to silver contacts to be 0.24 ± 0.11 Ω cm^2 (Figure 2b).

Consistent with other reports investigating the bulk conductivity of PEDOT:PSS, the addition of DMSO, EG, PEG, and glycerol all resulted in a decrease in bulk resistivity (i.e., an increase in conductivity) (Figure 2c). Notably, the bulk resistivity tended to steadily decrease relative to the additive loading, up until enough was added to saturate the secondary dopant effect throughout the bulk of the film. As such, 3 vol % glycerol, 3 vol % EG, and 5 vol % DMSO all result in very similar bulk resistivities (~10^{-3} Ω cm, or conductivities of ~1000 S cm^{-1}). However, further increasing the additive loading only marginally resulted in a continued decrease in bulk resistivity for DMSO (with the best bulk conductivity at 8 vol %). For these small polar molecules, the decrease in resistivity can mainly be attributed to changes in the film morphology (as previously discussed).[4,20,28,32,57] In contrast, blending with MWCNT (which increases conductivity as a conductive filler) resulted in a comparatively higher bulk resistivity of ~9 × 10^{-3} Ω cm at 1.5 wt %.

While polar small molecules outperformed MWCNT for bulk properties, PEDOT:PSS blended with 0.5 wt % MWCNT by far had the lowest contact resistivity (4.8 × 10^{-3} Ω cm^2) (Figure 2b). However, the contact resistivity increased while the bulk resistivity decreased as the loading of MWCNT increased (Figure S1), suggesting a tradeoff between the bulk and surface behaviors. The contact resistivity appeared to be relatively invariant on the MWCT diameter, as little change was observed when the MWCNT diameter was increased at a constant loading (Figure S2).

https://doi.org/10.1021/acsami.3c08341
ACS Appl. Mater. Interfaces 2023, 15, 38143−38153

Despite similarities in bulk properties between the polar small molecules, there were clear differences between the contact behaviors. Increasing the loading of EG steadily decreased the contact resistivity to $\sim 10^{-1}$ Ω cm^2 at 8 vol %. Increasing the loading of DMSO resulted in similar contact resistivities from 1 to 8 vol %, with a further decrease to $\sim 4 \times 10^{-2}$ Ω cm^2 at 10 vol %. Interestingly, the lowest contact resistivity for DMSO films (10 vol %) did not occur at the same loading as the lowest bulk resistivity (8 vol %). In contrast to DMSO and EG, lower loadings of glycerol seemed to result in better contact resistivities, with $\sim 3 \times 10^{-2}$ Ω cm^2 at 1 vol % and $\sim 5 \times 10^{-2}$ Ω cm^2 at 3−5 vol %. However, 1 vol % glycerol was insufficient to completely dope the bulk of the PEDOT:PSS film, resulting in a bulk resistivity of $\sim 5 \times 10^{-2}$ Ω cm (compared to $\sim 3 \times 10^{-3}$ Ω cm at 3 vol %). In contrast with the other additives, the incorporation of PEG resulted in an increase in contact resistivity (ca. 1−3 Ω cm^2), even though the bulk resistivity was decreased with respect to pristine PEDOT:PSS. We observed significant phase segregation in films of PEDOT:PSS/PEG, both from optical microscopy and from AFM height and phase plots, indicating large insulating domains of PEG at the surface of the film (Figures S3−S5, Table S2). Thus, we attribute the poor surface conductance of PEDOT:PSS/PEG films to an increase in insulating material (as PEG itself is electrically insulating) and large domains of insulating PEG at the PEDOT:PSS/silver interface.

Crosslinking the PEDOT:PSS film by increasing the loading of GOPS corresponded to an increase in both bulk resistivity (in agreement with previous studies[43,49]) and contact resistivity, which could be mostly recovered by the addition of secondary dopants (Figure 2d,e). While all three blends incorporating both GOPS and secondary dopants had similar bulk conductivities to films without crosslinker ($\sim 10^{-3}$ Ω cm), the contact resistivities were slightly increased ($\sim 7 \times 10^{-2}$ Ω cm^2). Interestingly, glycerol and EG seemed to outperform DMSO in restoring the contact conductance, despite the bulk conductivities being similar and the opposite being true (i.e., DMSO and glycerol outperform EG) when the PEDOT:PSS film was not crosslinked.

Most striking from these findings were (1) the low contact resistivity of PEDOT:PSS/MWCNT despite its high bulk resistance and (2) the differences in contact resistivities for the polar small molecule dopants despite their similarities in bulk resistivity. We use conductive AFM (c-AFM) to connect these measured decreases in the contact resistivity to changes to the surface morphology of PEDOT:PSS (Figure 3).

Conductive AFM measurements suggest significant differences in surface conductivity between pristine PEDOT:PSS films and PEDOT:PSS blended with additives (Figure 3a, Table S3, Figures S6−S10). Current plots in Figure 3a,c are visualized with the same scale bars in order to allow for simple comparison between samples but are shown with individual scale bars in Figures S6 and S7. Specifically, the average measured current for pristine PEDOT:PSS was <1 μA (Figure 3b); the addition of 10% DMSO, 5% glycerol, and 5% EG resulted in an average current of 6.5, 4.9, and 4.5 μA, respectively (Table S3). In general, these measurements correlated well to the measured contact resistivities of the films, where the DMSO film has the greatest conductance ($\sim 4 \times 10^{-2}$ Ω cm^2), followed by glycerol ($\sim 5 \times 10^{-2}$ Ω cm^2), and then by EG ($\sim 10^{-1}$ Ω cm^2) (Figure 2b). However, although 1 vol % glycerol resulted in the lowest contact resistivity of the doped PEDOT:PSS films, the measured current was relatively low due to the incomplete doping of the bulk film (as it is influenced by the through-film nature of the c-AFM measurement) (Figure S8). In contrast, the PEDOT:PSS/MWCNT film had the widest distribution of measured currents, with an average of 4.5 μA (Table S3). Large bright spots on the c-AFM image suggest the formation of large domains of MWCNT at the surface, while the rest of the film strongly resembles that of pristine PEDOT:PSS (Figure S6). The strong bi-modality of the PEDOT:PSS/MWCNT current histogram agrees with this observation, indicating domains of distinct phases of PEDOT:PSS and of MWCNTs. These MWCNT domains are highly conductive, resulting in the greatest fraction of pixels with a maximum measured current of 10 μA or greater (as limited by the resolution of the measurement). As such, these observations suggest that the low contact resistivity is due to favorable surface conductance through these MWCNT domains. Here, the MWCNT acts as a conductive filler rather than a secondary dopant (for which polar species are required). Phase segregation results in large domains of MWCNT within the film that promote charge transport, as the PEDOT:PSS domains are comparatively more insulting (due to no secondary doping effects resulting in a more favorable conduction pathway). The low loading of MWCNT within the film is unable to form highly percolated conduction pathways through the bulk, but the aggregated MWCNT at the surface facilitates surface conductance (Figure S10). As such, the contact resistivity of the 0.5 wt % MWCNT film is low while the bulk resistivity is high. It should be noted that no current plot is shown for PEDOT:PSS/PEG due to the largely insulating surface morphology resulting in poor measurements (e.g., due to charging leaving artifacts on the measured current plot). However, this observation was still in agreement with the contact resistivity measurements, as PEDOT:PSS/PEG was found to have a greater contact resistivity than pristine PEDOT:PSS by approximately a factor of 10. The incorporation of PEG was also found to significantly soften the film, resulting in the cantilever probe often scratching through to the silicon substrate and short-circuiting the measurement (Figure S6).

Crosslinking the PEDOT:PSS film with GOPS significantly increased the amount of insulating material in the solid film, and thus greatly decreased the measured current. Chains of PSS become covalently bound to the silane crosslinker, resulting in different morphological changes induced by the incorporation of a secondary dopant. The surface resulting from crosslinking PEDOT:PSS with 1 vol % GOPS was highly insulating, and thus did not yield measurements with measurable currents (i.e., resembling that of PEDOT:PSS/PEG) (Figure 3c,d). However, as suggested by TLM measurements, adding secondary dopants can partially recover its conductivity. Specifically, the addition of DMSO to the crosslinked PEDOT:PSS film results in small specks of bright regions in the current plot, although the majority of the film is still highly insulating (Figure S7). In contrast, the addition of EG shows a highly speckled current plot, likely suggesting highly conductive pathways dispersed throughout the morphology of the crosslinked film. Finally, the addition of glycerol results in significant phase separation, with large domains of dark and bright regions. As such, the average measured current of the glycerol blended films is the greatest (Table S3, Figure S7). These findings correspond well to the TLM measurements, which showed that the addition of glycerol and EG resulted in lower contact resistivities than that

https://doi.org/10.1021/acsami.3c08341
ACS Appl. Mater. Interfaces 2023, 15, 38143−38153

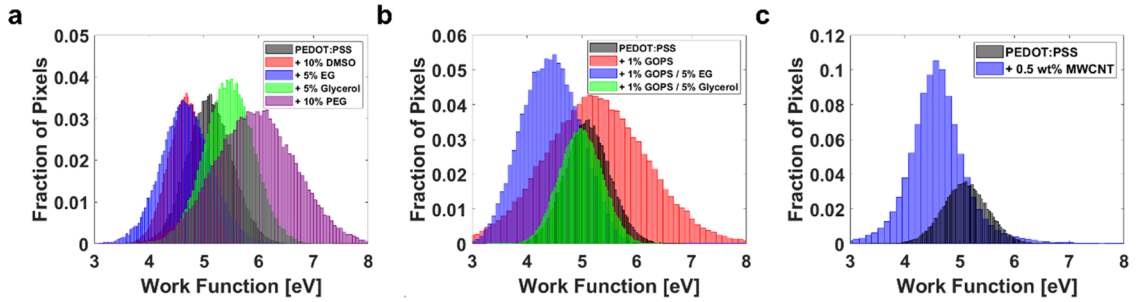

Figure 4. Work function histograms of representative PEDOT:PSS films as measured by KPFM. PEDOT:PSS blended with (a) three secondary dopants (DMSO, EG, glycerol) and one polymer dopant (PEG), (b) crosslinked with GOPS and blended with EG or glycerol, and (c) blended with MWCNT. No measurements could be collected for PEDOT:PSS/GOPS/DMSO.

of DMSO for crosslinked films (Figure 2d). However, the measured current for all crosslinked films was significantly lower than that of their non-crosslinked counterparts, which explains why the non-crosslinked films had lower contact resistivities.

As charge transfer across an interface is dependent on the alignment/mismatch of the energetics of the two materials, the work function of each PEDOT:PSS film was then measured using KPFM (Figure 4, Table 1, Figure S11) and UPS (as extracted from the secondary electron cut-off (SECO)) (Table 1, Figure S12). In addition to these measurements, we used XPS to compare the ratio of PSS to PEDOT of each representative film to estimate the ratio of conductive species at the surface (Table 1, Figure S13).

Table 1. Electronic Properties Associated with the Surface Morphology of Representative PEDOT:PSS Films as Extracted by KPFM (Work Function), UPS (Work Function), and XPS (Ratio of PSS to PEDOT)

	KPFM	UPS	XPS
material	work function [eV][c]	work function [eV]	PSS:PEDOT ratio
PEDOT:PSS (Clevios PH1000)	5.1 ± 0.41	4.72	2.87
+ 10 vol % DMSO	4.68 ± 0.33	4.78	2.58
+ 5 vol % EG	4.67 ± 0.46	4.96	2.55
+ 5 vol % glycerol	5.45 ± 0.45	4.79	2.37
+ 10 vol % PEG	5.94 ± 0.73	[a]	[a]
+ 0.5 wt % MWCNT	4.59 ± 0.66	4.96	2.21
+ 1 vol % GOPS	5.24 ± 0.97	4.29	1.96
+ 1 vol % GOPS + 10 vol % DMSO	[b]	4.42	1.82
+ 1 vol % GOPS + 5 vol % EG	4.43 ± 0.53	4.42	2.47
+ 1 vol % GOPS + 5 vol % glycerol	4.98 ± 0.38	4.30	1.93

[a]Energetics unable to be accurately determined due to charging of the sample during measurement during XPS/UPS. [b]Work function unable to be accurately extracted from KPFM due to poor measurement quality, likely due to charging at the insulating surface. [c]Error reported as standard deviation.

KPFM measurements largely agreed with previous studies on the energetics of PEDOT:PSS, which have observed that the addition of DMSO[58] or EG[59] into the solid film can result in a decrease in the work function (with glycerol having conflicting reports[60,61]). Here, both doped films measured an average work function of 4.7 eV, compared to the work function of pristine PEDOT:PSS at 5.1 eV and PEDOT:PSS/glycerol at 5.4 eV. Likewise, KPFM of the PEDOT:PSS/MWCNT film measured a work function of ∼4.6 eV, which is in agreement with previous reports determining the work function of carbon nanotubes to range between 4.5 and 5 eV.[62,63] The work function of silver is typically measured to be 4.26 eV (we measure the work function by KPFM to be ∼4.37 eV, Figure S11), and thus a decrease in work function reduces the mismatch at the PEDOT:PSS/silver interface. Likewise, KPFM measurements suggest that the addition of GOPS tends to lower the work function of the PEDOT:PSS film, as the crosslinked PEDOT:PSS/EG and PEDOT:PSS/glycerol films both had lower work functions than their non-crosslinked counterparts.

Trends in UPS measurements were consistent with those in KPFM measurements, agreeing that the addition of GOPS tends to lower the work function. As such, crosslinked PEDOT:PSS films blended with DMSO (4.4 eV), EG (4.4 eV), and glycerol (4.3 eV) all had lower work functions than their non-crosslinked counterparts. A decreased mismatch in band alignment would explain the relatively recovered contact resistivity for crosslinked films blended with secondary dopants, despite c-AFM showing significantly decreased surface conductance. In contrast, the addition of 10 vol % PEG results in the highest measured work function (∼6 eV). Thus, a significant increase in energetic mismatch likely contributes to the high contact resistivity of PEDOT:PSS/PEG films.

To better understand how the various additives affected the surface composition of PEDOT:PSS, S 2p XPS scans were used to extract the ratio of PSS to PEDOT within 8 nm of the surface (Figure S13). We found that pristine PEDOT:PSS had the greatest ratio of PSS to PEDOT (2.87:1), while the addition of DMSO, EG, or glycerol resulted in a decreased ratio of 2.58, 2.55, or 2.37, respectively. This finding is in agreement with previous results from the literature[2,64] and explains the decrease in measured contact resistivity, as only the PEDOT species are electrically conductive. Interestingly, all crosslinked films showed a similar decrease in PSS to PEDOT ratio, including PEDOT:PSS/GOPS/DMSO, which had a ratio of 1.82 (suggesting a relatively high proportion of PEDOT chains at the surface). However, the c-AFM measurements showed very little through-film current in the current plot, despite a relatively low bulk and contact resistivity (at least, significantly lower than pristine PEDOT:PSS).

Finally, while qualitative trends remained consistent across both UPS and KPFM methods, we aim to reconcile

https://doi.org/10.1021/acsami.3c08341
ACS Appl. Mater. Interfaces 2023, 15, 38143−38153

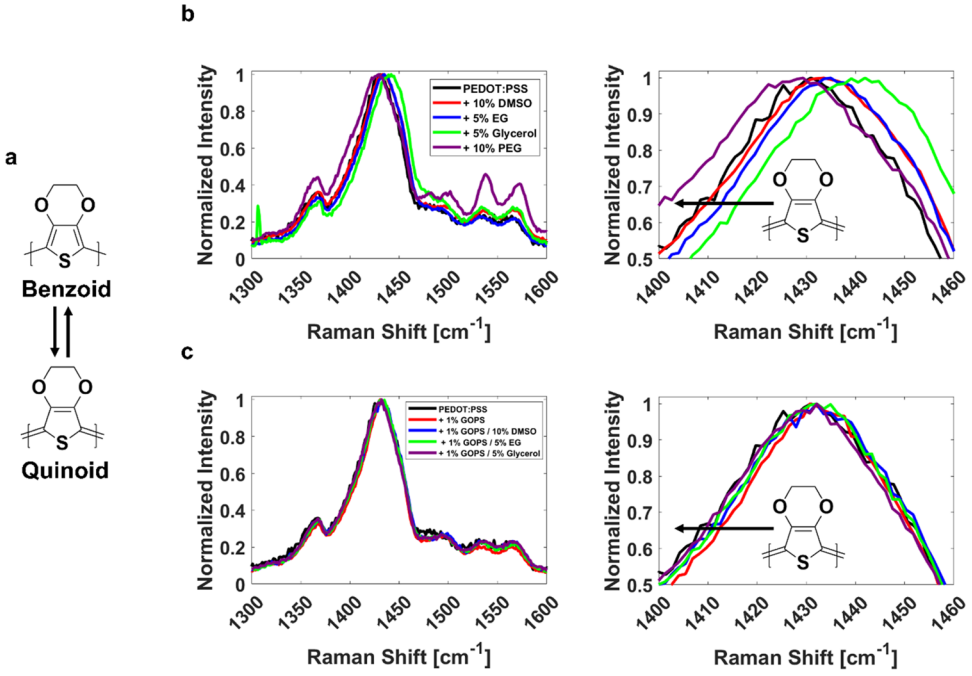

Figure 5. (a) Raman spectroscopy is used to qualitatively observe shifts associated with benzoid or quinoid structures. Spectra comparing the Raman shift of (b) PEDOT:PSS films blended with dopants (DMSO, EG, PEG, glycerol) and (c) PEDOT:PSS films crosslinked with GOPS as averaged from three measured spectra. Shown on the right of (b) and (c) are zoomed-in plots of spectra associated with the thiophene ring on PEDOT:PSS.

quantitative differences between measurements of work function from samples of the same condition. Likewise, we aim to elucidate the surface composition of the PEDOT:PSS film. Here, an increase in work function generally suggests an increased presence of PSS, and a decreased work function suggests an increased presence of PEDOT.[65] For example, the pristine PEDOT:PSS film had a work function of 5.1 eV via KPFM and a work function of 4.7 eV via UPS. Likewise, UPS measured the work function of doped films to be similar to pristine PEDOT:PSS and slightly increased for PEDOT:PSS/EG, whereas KPFM measured PEDOT:PSS/EG and PEDOT:PSS/DMSO to have lower work functions compared to pristine PEDOT:PSS. Additionally, there were significant differences between the PEDOT:PSS/GOPS films, where KPFM measured the mean work function to be 5.2 eV and UPS to be 4.3 eV. Work by Lee and Chung has shown that vapor treatment with DMSO can drive phase segregation of PEDOT and PSS domains at the surface, resulting in a concentration of PSS in the top several nanometers of the film and thus increasing the work function as measured by UPS.[65] Moreover, as previously discussed, other studies have shown that blending with secondary dopants resulted in similar phase segregation throughout the bulk of the film.[4] Thus, these discrepancies are consistent with the different depth sensitivities of the measurements. Specifically, KPFM employs a through-film measurement with depth resolution up to several hundred nanometers and a decreasing spatial resolution relative to an increase in depth,[66] whereas UPS is highly sensitive to the surface, with a depth resolution of 2−3 nm. Thus, KPFM measurements are consistent with a decrease in work function due to the phase-segregated morphology of the bulk. In contrast, UPS measures an increase in work function, likely from an increase in PSS at the surface of the film due to phase segregation (particularly for doping with EG). However, XPS, with a depth resolution of ∼8 nm, suggests that doping PEDOT:PSS results in a decreased PSS to PEDOT ratio (i.e., an increase in the proportion of PEDOT) relative to the pristine film. A plausible explanation (consistent with the literature[2,20,67,68]) is that secondary doping effects result in a thin and confined layer of PSS at the surface of the PEDOT:PSS film (within 0−3 nm), and phase segregation resulting in larger, PEDOT-rich domains below the confined PSS layer (i.e., within 3−8 nm of the surface and throughout the bulk). As a result, the signal from the top ∼3 nm (i.e., UPS) appears PSS-rich while the signals from the top ∼8 nm and below (i.e., XPS and KPFM) appear PEDOT-rich.

Lastly, we compare the benzoid-to-quinoid ratios that comprise the PEDOT:PSS at the surface of each film using Raman spectroscopy (Figure 5).

In a solid film, PEDOT moieties that form the polymer chain are understood to resonate between benzoid and quinoid structures as a result of charge transfer along the backbone (Figure 5a).[5,69] The addition of polar dopants has been shown to increase the proportion of quinoid species to benzoid species, resulting in conformational changes to the PEDOT backbone.[70] In particular, the polymer chain uncoils due to the change in chemical structure, resulting in a more linear PEDOT backbone. As such, this increase in backbone planarity allows for more efficient charge delocalization and likely greater intermolecular interactions (e.g., π-stacking, chain packing) within PEDOT-rich domains, thus resulting in increased charge transport (i.e., conductivity).[5,69] To characterize the benzoid−quinoid conformations present, we measured the Raman shift associated with the symmetric $C_\alpha{=}C_\beta$ stretching of the thiophene ring around 1450 cm^{-1} for pristine PEDOT:PSS.[69] Only PEDOT:PSS/PEG showed a noticeable peak shift at 1410−1420 cm^{-1} (i.e., a lower-frequency shift), as well as a broadening of the peak, suggesting a greater proportion of quinoid structures compared to that of pristine PEDOT:PSS (Figure 5b). In contrast, DMSO and EG

https://doi.org/10.1021/acsami.3c08341
ACS Appl. Mater. Interfaces 2023, 15, 38143−38153

showed relatively similar spectra to pristine PEDOT:PSS, albeit a modest shift to a higher frequency at 1440−1450 cm^{-1}, which likely indicates a greater proportion of benzoid structures. Finally, glycerol showed a significant shift to a higher frequency and thus likely the greatest proportion of benzoid structures. Additionally, we find that crosslinking the PEDOT:PSS film results in a slight shift to a higher frequency in the Raman spectra, although the addition of DMSO, EG, or glycerol all essentially restore the ratio of structural variants to that of pristine PEDOT:PSS (Figure 5c). No qualitative observations could be made for PEDOT:PSS/MWCNT films, as the shift associated with the MWCNT overlap with that of PEDOT:PSS (Figure S14).

Other studies reporting a significantly favorable shift in quinoid transformation typically incorporated a surface treatment (e.g., dipping a doped film in EG[69] or aqueous DMSO[19]), which likely increases the polar interactions necessary to promote the structural transformation at the surface. Our findings suggest that blending PEDOT:PSS with a dopant does not necessarily achieve the same increase in quinoid moieties at the surface, but can easily be promoted by post-treatment. As such, we likely expect a surface treatment to further increase the surface conductivity of PEDOT:PSS films. For example, Kirihara et al. reported that an additional EG surface treatment decreased the contact resistivity of doped PEDOT:PSS films from ∼2 × 10^{-2} Ω cm^{-2} to ∼1 × 10^{-2} Ω cm^{-2}.[12] The authors hypothesized that this reduction was due to an increase in contact area, as the surface treatment created a wavy topography. However, together, our observations suggest that an additional factor in this reported reduction in contact resistivity was possibly due to an increase in quinoid species as the surface. In contrast, in this work, changes to the work function and surface composition were likely far greater determinants for the contact properties.

CONCLUSIONS

The bulk conductivity of PEDOT:PSS is typically increased by blending with secondary dopants or conductive filler. We show that these additives also reduce the contact resistance by modifying the surface morphology, composition, and energetics of the solid film, and thus offer an avenue for tuning the contact behavior. Blending with small amounts of MWCNT resulted in highly conductive domains at the surface of the PEDOT:PSS film and the lowest contact resistivity reported in this study (4.8 × 10^{-3} Ω cm^2), which appears to be the lowest contact resistivity for PEDOT:PSS reported so far. However, the bulk resistivities of MWCNT films were all higher than that of doped films due to the lack of secondary dopant effects benefiting the morphology of PEDOT:PSS domains. When polar small molecule dopants were added, a reduction in contact resistance is typically correlated with a decrease in PSS to PEDOT ratio decreases, a decrease in work function (except in the case of glycerol), and an increase in phase segregation (as noted by other studies elucidating bulk morphology). Here, 1 vol % glycerol results in the lowest contact resistivity (∼3 × 10^{-2} Ω cm^2), but 10 vol % DMSO results in the best combination of low contact resistivity (∼4 × 10^{-2} Ω cm^2) as well as low bulk resistivity (∼3 × 10^{-3} Ω cm^2). Other studies have shown that surface treatment of PEDOT:PSS films with ethylene glycol or dimethyl sulfoxide can promote a favorable transformation of benzoid-to-quinoid structures, which can also promote a decrease in contact resistance. When the PEDOT:PSS film is crosslinked with an insulating silane crosslinker, the contact resistance dramatically increases due to the increase in insulating material within the film. However, 5 vol % EG or glycerol can be incorporated to recover the contact resistance, which again stems from a decrease in work function, decrease in PSS to PEDOT ratio, and increase in phase-segregated morphology that allows for the formation of conductive pathways. We summarize the changes in surface properties that reduce the contact resistance of PEDOT:PSS films (Figure 6).

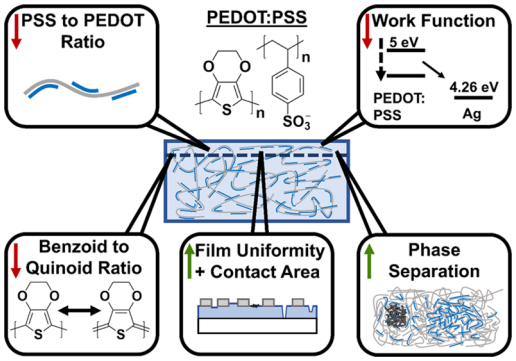

Figure 6. Changes to the surface properties of PEDOT:PSS films induced by incorporation of additives (DMSO, EG, PEG, glycerol, MWCNT, GOPS) resulting in a reduction in contact resistance to silver contacts. The contact resistivity is reduced by decreasing the ratio of PSS to PEDOT at the surface, decreasing the work function for more favorable band alignment with silver, decreasing the benzoid-to-quinoid ratio by surface treatment, increasing the film uniformity and contact area, and increasing the phase separation (induced by blending in electronic filler or secondary dopant effects).

Reduction of the contact resistance between layers within a device stack can improve the electronic function of several applications employing semiconducting polymer films. As such, contact resistance is a crucial consideration for device stacks made of ultrathin films or where electronic properties are dominated by charge injection rather than transfer through an active layer. Two examples of such applications are organic field effect transistors and charge injection layers in perovskite or organic solar cells. However, the contact resistance is governed by a conglomerate of physical phenomena occurring at the interface of two materials in contact, ranging from the chemical structures to how they are processed, which often requires a detailed investigation of the film morphology, composition, and energetics. Likewise, in this study, we often observed tradeoffs between the bulk and contact properties of PEDOT:PSS films, particularly those blended with MWCNT or doped with secondary dopants. We expect further reduction of the contact resistivity of PEDOT:PSS can be made possible by combining different strategies mentioned in this work. For example, replacing multi-walled carbon nanotubes with their single-walled counterparts (which have far greater conductivity), blending both CNT and secondary dopants within the film, or surface treatment of the PEDOT:PSS film (e.g., spray coating with CNTs, EG, or DMSO). Thus, a detailed understanding of structure−property and process−property relationships, and how they affect the morphology of the resulting film, offers an avenue for the rational design of devices incorporating ultrathin PEDOT:PSS films.

https://doi.org/10.1021/acsami.3c08341
ACS Appl. Mater. Interfaces 2023, 15, 38143−38153

■ ASSOCIATED CONTENT

Supporting Information

The Supporting Information is available free of charge at https://pubs.acs.org/doi/10.1021/acsami.3c08341.

Experimental methods, SEM images, effect of MWCNT loading on electronic properties, AFM height plots and film roughness, c-AFM current plots, KPFM work function plots, SECO values, XPS spectra and curve fitting, and Raman spectra (PDF)

■ AUTHOR INFORMATION

Corresponding Authors

David P. Fenning − *Department of NanoEngineering, University of California, San Diego, La Jolla, California 92093-0448, United States;* orcid.org/0000-0002-4609-9312; Email: dfenning@ucsd.edu

Darren J. Lipomi − *Department of NanoEngineering, University of California, San Diego, La Jolla, California 92093-0448, United States;* orcid.org/0000-0002-5808-7765; Email: dlipomi@ucsd.edu

Authors

Alexander X. Chen − *Department of NanoEngineering, University of California, San Diego, La Jolla, California 92093-0448, United States;* orcid.org/0000-0003-1919-6755

Guillermo L. Esparza − *Department of NanoEngineering, University of California, San Diego, La Jolla, California 92093-0448, United States*

Ignasi Simon − *Department of NanoEngineering, University of California, San Diego, La Jolla, California 92093-0448, United States*

Sean P. Dunfield − *Department of NanoEngineering, University of California, San Diego, La Jolla, California 92093-0448, United States*

Yi Qie − *Department of NanoEngineering, University of California, San Diego, La Jolla, California 92093-0448, United States*

Jordan A. Bunch − *Department of NanoEngineering, University of California, San Diego, La Jolla, California 92093-0448, United States*

Rachel Blau − *Department of NanoEngineering, University of California, San Diego, La Jolla, California 92093-0448, United States*

Allison Lim − *Department of NanoEngineering, University of California, San Diego, La Jolla, California 92093-0448, United States*

Henry Zhang − *Department of NanoEngineering, University of California, San Diego, La Jolla, California 92093-0448, United States*

Sarah E. Brew − *Department of NanoEngineering, University of California, San Diego, La Jolla, California 92093-0448, United States*

Finnian M. O'Neill − *Department of NanoEngineering, University of California, San Diego, La Jolla, California 92093-0448, United States*

Complete contact information is available at: https://pubs.acs.org/10.1021/acsami.3c08341

Notes

The authors declare no competing financial interest.

■ ACKNOWLEDGMENTS

This work was supported by the Air Force Office of Scientific Research (AFOSR) grant no. FA9550-22-1-0454 to D.J.L. and by the California Energy Commission (CEC) grant no. EPC-19-004 to D.P.F. A.X.C. acknowledges support from the UC President's Dissertation Year Fellowship. G.L.E. acknowledges support from the UC San Diego Materials Science and Engineering Dissertation Year Fellowship. R.B. acknowledges support from the Zuckerman-CHE STEM Leadership Program and Marie Skłodowska-Curie Actions (MSCA) fellowship. The authors acknowledge the use of facilities and instrumentation supported by NSF through the UC San Diego Materials Research Science and Engineering Center (UCSD MRSEC), grant DMR-2011924. This work was performed in part at the San Diego Nanotechnology Infrastructure (SDNI) of UC San Diego, a member of the National Nanotechnology Coordinated Infrastructure, which is supported by the National Science Foundation (Grant ECCS-2025752). The authors thank Conor Holzhall for his support with c-AFM and KPFM measurements, Dr. Ich Tran for his support with XPS and UPS measurements, and Prof. Laure Kayser for helpful discussions.

■ REFERENCES

(1) Gueye, M. N.; Carella, A.; Faure-Vincent, J.; Demadrille, R.; Simonato, J. P. Progress in Understanding Structure and Transport Properties of PEDOT-Based Materials: A Critical Review. *Prog. Mater. Sci.* **2020**, *108*, No. 100616.

(2) Jönsson, S.; Birgerson, J.; Crispin, X.; Greczynski, G.; Osikowicz, W.; Denier van der Gon, A. W.; Salaneck, W. R.; Fahlman, M. The Effects of Solvents on the Morphology and Sheet Resistance in Poly(3,4-Ethylenedioxythiophene)-Polystyrenesulfonic Acid (PEDOT-PSS) Films. *Synth. Met.* **2003**, *139*, 1−10.

(3) Shi, H.; Liu, C.; Jiang, Q.; Xu, J. Effective Approaches to Improve the Electrical Conductivity of PEDOT:PSS: A Review. *Adv. Electron. Mater.* **2015**, *1*, No. 1500017.

(4) Nevrela, J.; Micjan, M.; Novota, M.; Kovacova, S.; Pavuk, M.; Juhasz, P.; Kovac, J.; Jakabovic, J.; Weis, M. Secondary Doping in Poly(3,4-Ethylenedioxythiophene):Poly(4-Styrenesulfonate) Thin Films. *J. Polym. Sci., Part B: Polym. Phys.* **2015**, *53*, 1139−1146.

(5) Ouyang, J. "Secondary Doping" Methods to Significantly Enhance the Conductivity of PEDOT:PSS for Its Application as Transparent Electrode of Optoelectronic Devices. *Displays* **2013**, *34*, 423−436.

(6) Kayser, L. V.; Lipomi, D. J. Stretchable Conductive Polymers and Composites Based on PEDOT and PEDOT:PSS. *Adv. Mater.* **2019**, *31*, No. 1806133.

(7) Onorato, J. W.; Luscombe, C. K. Morphological Effects on Polymeric Mixed Ionic/Electronic Conductors. *Mol. Syst. Des. Eng.* **2019**, *4*, 310−324.

(8) Reeves, G. K.; Harrison, H. B. Obtaining the Specific Contact Resistance from Transmission Line Model Measurements. *IEEE Electron Device Lett.* **1982**, *3*, 111−113.

(9) Robertson, J. Band Offsets, Schottky Barrier Heights, and Their Effects on Electronic Devices. *J. Vac. Sci. Technol., A* **2013**, *31*, No. 050821.

(10) Waldrip, M.; Jurchescu, O. D.; Gundlach, D. J.; Bittle, E. G. Contact Resistance in Organic Field-Effect Transistors: Conquering the Barrier. *Adv. Funct. Mater.* **2020**, *30*, No. 1904576.

(11) Klauk, H. Will We See Gigahertz Organic Transistors? *Adv. Electron. Mater.* **2018**, *4*, No. 1700474.

(12) Kirihara, K.; Wei, Q.; Mukaida, M.; Ishida, T. Reduction of Specific Contact Resistance between the Conducting Polymer PEDOT:PSS and a Metal Electrode by Addition of a Second Solvent during Film Formation and a Post-Surface Treatment. *Synth. Met.* **2018**, *246*, 289−296.

(13) Crinon, E.; Evans, J. T. The Effect of Surface Roughness, Oxide Film Thickness and Interfacial Sliding on the Electrical Contact Resistance of Aluminium. *Mater. Sci. Eng. A* **1998**, *242*, 121−128.
(14) Kim, C. H.; Bonnassieux, Y.; Horowitz, G. Charge Distribution and Contact Resistance Model for Coplanar Organic Field-Effect Transistors. *IEEE Trans. Electron Devices* **2013**, *60*, 280−287.
(15) Wang, S. D.; Minari, T.; Miyadera, T.; Aoyagi, Y.; Tsukagoshi, K. Bias Stress Instability in Pentacene Thin Film Transistors: Contact Resistance Change and Channel Threshold Voltage Shift. *Appl. Phys. Lett.* **2008**, *92*, No. 061101.
(16) Liu, C.; Xu, Y.; Li, Y.; Scheideler, W.; Minari, T. Critical Impact of Gate Dielectric Interfaces on the Contact Resistance of High-Performance Organic Field-Effect Transistors. *J. Phys. Chem. C* **2013**, *117*, 12337−12345.
(17) Smith, J.; Hamilton, R.; Qi, Y.; Kahn, A.; Bradley, D. D. C.; Heeney, M.; McCulloch, I.; Anthopoulos, T. D. The Influence of Film Morphology in High-Mobility Small-Molecule: Polymer Blend Organic Transistors. *Adv. Funct. Mater.* **2010**, *20*, 2330−2337.
(18) Crispin, X.; Marciniak, S.; Osikowicz, W.; Zotti, G.; Gon, A. W. D. V. A. N. D. E. R.; Louwet, F.; Fahlman, M.; Groenendaal, L.; Schryver, F. D. E.; Salaneck, W. R. Conductivity, Morphology, Interfacial Chemistry, and Stability of Poly (3,4-Ethylene Dioxythiophene)− Poly(Styrene Sulfonate): A Photoelectron Spectroscopy Study. *J. Polym. Sci., Part B: Polym. Phys.* **2003**, *41*, 2561−2583.
(19) Deetuam, C.; Weise, D.; Samthong, C.; Praserthdam, P.; Baumann, R. R.; Somwangthanaroj, A. Electrical Conductivity Enhancement of Spin-Coated PEDOT:PSS Thin Film via Dipping Method in Low Concentration Aqueous DMSO. *J. Appl. Polym. Sci.* **2015**, *132*, No. 42108.
(20) Crispin, X.; Jakobsson, F. L. E.; Crispin, A.; Grim, P. C. M.; Andersson, P.; Volodin, A.; Van Haesendonck, C.; Van Der Auweraer, M.; Salaneck, W. R.; Berggren, M. The Origin of the High Conductivity of Poly(3,4-Ethylenedioxythiophene)- Poly-(Styrenesulfonate) (PEDOT-PSS) Plastic Electrodes. *Chem. Mater.* **2006**, *18*, 4354−4360.
(21) Hokazono, M.; Anno, H.; Toshima, N. Thermoelectric Properties and Thermal Stability of PEDOT:PSS Films on a Polyimide Substrate and Application in Flexible Energy Conversion Devices. *J. Electron. Mater.* **2014**, *43*, 2196−2201.
(22) Lim, K.; Jung, S.; Lee, S.; Heo, J.; Park, J.; Kang, J. W.; Kang, Y. C.; Kim, D. G. The Enhancement of Electrical and Optical Properties of PEDOT:PSS Using One-Step Dynamic Etching for Flexible Application. *Org. Electron.* **2014**, *15*, 1849−1855.
(23) Lee, S. H.; Park, H.; Son, W.; Choi, H. H.; Kim, J. H. Novel Solution-Processable, Dedoped Semiconductors for Application in Thermoelectric Devices. *J. Mater. Chem. A* **2014**, *2*, 13380−13387.
(24) Kim, N.; Kee, S.; Lee, S. H.; Lee, B. H.; Kahng, Y. H.; Jo, Y. R.; Kim, B. J.; Lee, K. Highly Conductive PEDOT:PSS Nanofibrils Induced by Solution-Processed Crystallization. *Adv. Mater.* **2014**, *26*, 2268−2272.
(25) Diah, A. W. M.; Quirino, J. P.; Belcher, W.; Holdsworth, C. I. An Assessment of the Effect of Synthetic and Doping Conditions on the Processability and Conductivity of Poly(3,4-Ethylenedioxythiophene)/Poly(Styrene Sulfonic Acid). *Macromol. Chem. Phys.* **2016**, *217*, 1907−1916.
(26) Blau, R.; Chen, A. X.; Polat, B.; Becerra, L. L.; Runser, R.; Zamanimeymian, B.; Choudhary, K.; Lipomi, D. J. Intrinsically Stretchable Block Copolymer Based on PEDOT:PSS for Improved Performance in Bioelectronic Applications. *ACS Appl. Mater. Interfaces* **2022**, *14*, 4823−4835.
(27) Kayser, L. V.; Russell, M. D.; Rodriquez, D.; Abuhamdieh, S. N.; Dhong, C.; Khan, S.; Stein, A. N.; Ramírez, J.; Lipomi, D. J. RAFT Polymerization of an Intrinsically Stretchable Water-Soluble Block Copolymer Scaffold for PEDOT. *Chem. Mater.* **2018**, *30*, 4459−4468.
(28) Rivnay, J.; Inal, S.; Collins, B. A.; Sessolo, M.; Stavrinidou, E.; Strakosas, X.; Tassone, C.; Delongchamp, D. M.; Malliaras, G. G. Structural Control of Mixed Ionic and Electronic Transport in Conducting Polymers. *Nat. Commun.* **2016**, *7*, No. 11287.
(29) Kim, S. M.; Kim, C. H.; Kim, Y.; Kim, N.; Lee, W. J.; Lee, E. H.; Kim, D.; Park, S.; Lee, K.; Rivnay, J.; Yoon, M. H. Influence of PEDOT:PSS Crystallinity and Composition on Electrochemical Transistor Performance and Long-Term Stability. *Nat. Commun.* **2018**, *9*, No. 3858.
(30) Timpanaro, S.; Kemerink, M.; Touwslager, F. J.; De Kok, M. M.; Schrader, S. Morphology and Conductivity of PEDOT/PSS Films Studied by Scanning-Tunneling Microscopy. *Chem. Phys. Lett.* **2004**, *394*, 339−343.
(31) Alemu Mengistie, D.; Wang, P. C.; Chu, C. W. Effect of Molecular Weight of Additives on the Conductivity of PEDOT:PSS and Efficiency for ITO-Free Organic Solar Cells. *J. Mater. Chem. A* **2013**, *1*, 9907−9915.
(32) Palumbiny, C. M.; Liu, F.; Russell, T. P.; Hexemer, A.; Wang, C.; Müller-Buschbaum, P. The Crystallization of PEDOT:PSS Polymeric Electrodes Probed in Situ during Printing. *Adv. Mater.* **2015**, *27*, 3391−3397.
(33) Lo, C.-Y.; Wu, Y.; Awuyah, E.; Meli, D.; Nguyen, D. M.; Wu, R.; Xu, B.; Strzalka, J.; Rivnay, J.; Martin, D. C.; Kayser, L. V. Influence of the Molecular Weight and Size Distribution of PSS on Mixed Ionic-Electronic Transport in PEDOT:PSS. *Polym. Chem.* **2022**, *13*, 2764−2775.
(34) Oechsle, A. L.; Heger, J. E.; Li, N.; Yin, S.; Bernstorff, S.; Müller-Buschbaum, P. Correlation of Thermoelectric Performance, Domain Morphology and Doping Level in PEDOT:PSS Thin Films Post-Treated with Ionic Liquids. *Macromol. Rapid Commun.* **2021**, *42*, No. 2170067.
(35) Dong, J.; Portale, G. Role of the Processing Solvent on the Electrical Conductivity of PEDOT:PSS. *Adv. Mater. Interfaces* **2020**, *7*, No. 2000641.
(36) Dauzon, E.; Mansour, A. E.; Niazi, M. R.; Munir, R.; Smilgies, D. M.; Sallenave, X.; Plesse, C.; Goubard, F.; Amassian, A. Conducting and Stretchable PEDOT:PSS Electrodes: Role of Additives on Self-Assembly, Morphology, and Transport. *ACS Appl. Mater. Interfaces* **2019**, *11*, 17570−17582.
(37) Hegde, R.; Ramji, K.; Peravali, S.; Shiralgi, Y.; Hegde, G.; Bathini, L. Characterization of MWCNT-PEDOT: PSS Nanocomposite Flexible Thin Film for Piezoresistive Strain Sensing Application. *Adv. Polym. Technol.* **2019**, *2019*, 1−9.
(38) Mannayil, J.; Methattel Raman, S.; Sankaran, J.; Raman, R.; Madambi Kunjukutan Ezhuthachan, J. Solution Processable PEDOT:PSS/Multiwalled Carbon Nanotube Composite Films for Flexible Electrode Applications. *Phys. Status Solidi A* **2018**, *215*, No. 1701003.
(39) Zhao, D.; Zhang, Q.; Chen, W.; Yi, X.; Liu, S.; Wang, Q.; Liu, Y.; Li, J.; Li, X.; Yu, H. Highly Flexible and Conductive Cellulose-Mediated PEDOT:PSS/MWCNT Composite Films for Supercapacitor Electrodes. *ACS Appl. Mater. Interfaces* **2017**, *9*, 13213−13222.
(40) Kim, J. Y.; Lee, W.; Kang, Y. H.; Cho, S. Y.; Jang, K. S. Wet-Spinning and Post-Treatment of CNT/PEDOT:PSS Composites for Use in Organic Fiber-Based Thermoelectric Generators. *Carbon* **2018**, *133*, 293−299.
(41) Liu, S.; Li, H.; He, C. Simultaneous Enhancement of Electrical Conductivity and Seebeck Coefficient in Organic Thermoelectric SWNT/PEDOT:PSS Nanocomposites. *Carbon* **2019**, *149*, 25−32.
(42) Singh, V.; Arora, S.; Arora, M.; Sharma, V.; Tandon, R. P. Characterization of Doped PEDOT: PSS and Its Influence on the Performance and Degradation of Organic Solar Cells. *Semicond. Sci. Technol.* **2014**, *29*, No. 045020.
(43) Håkansson, A.; Han, S.; Wang, S.; Lu, J.; Braun, S.; Fahlman, M.; Berggren, M.; Crispin, X.; Fabiano, S. Effect of (3-Glycidyloxypropyl)Trimethoxysilane (GOPS) on the Electrical Properties of PEDOT:PSS Films. *J. Polym. Sci., Part B: Polym. Phys.* **2017**, *55*, 814−820.
(44) Mantione, D.; Del Agua, I.; Schaafsma, W.; Elmahmoudy, M.; Uguz, I.; Sanchez-Sanchez, A.; Sardon, H.; Castro, B.; Malliaras, G. G.; Mecerreyes, D. Low-Temperature Cross-Linking of PEDOT:PSS

Films Using Divinylsulfone. *ACS Appl. Mater. Interfaces* **2017**, *9*, 18254−18262.
(45) Solazzo, M.; Krukiewicz, K.; Zhussupbekova, A.; Fleischer, K.; Biggs, M. J.; Monaghan, M. G. PEDOT:PSS Interfaces Stabilised Using a PEGylated Crosslinker Yield Improved Conductivity and Biocompatibility. *J. Mater. Chem. B* **2019**, *7*, 4811−4820.
(46) Duc, C.; Malliaras, G. G.; Senez, V.; Vlandas, A. Long-Term Ageing of PEDOT:PSS: Wettability Study. *Synth. Met.* **2018**, *238*, 14−21.
(47) ElMahmoudy, M.; Inal, S.; Charrier, A.; Uguz, I.; Malliaras, G. G.; Sanaur, S. Tailoring the Electrochemical and Mechanical Properties of PEDOT:PSS Films for Bioelectronics. *Macromol. Mater. Eng.* **2017**, *302*, No. 1600497.
(48) Gao, L.; Zhang, Z. G.; Xue, L.; Min, J.; Zhang, J.; Wei, Z.; Li, Y. All-Polymer Solar Cells Based on Absorption-Complementary Polymer Donor and Acceptor with High Power Conversion Efficiency of 8.27%. *Adv. Mater.* **2016**, *28*, 1884−1890.
(49) Zhang, S.; Kumar, P.; Nouas, A. S.; Fontaine, L.; Tang, H.; Cicoira, F. Solvent-Induced Changes in PEDOT:PSS Films for Organic Electrochemical Transistors. *APL Mater.* **2015**, *3*, No. 014911.
(50) Mak, L. K.; Rogers, C. M.; Northrop, D. C. Specific Contact Resistance Measurements on Semiconductors. *J. Phys. E* **1989**, *22*, 317−321.
(51) Pretl, S.; Hamacek, A.; Reboun, J.; Stulik, J.Contact Properties of PEDOT: PSS. In *4th Electronic System-Integration Technology Conference* 2012; pp 1−6.
(52) Hoppe, H.; Seeland, M.; Muhsin, B. Optimal Geometric Design of Monolithic Thin-Film Solar Modules: Architecture of Polymer Solar Cells. *Sol. Energy Mater. Sol. Cells* **2012**, *97*, 119−126.
(53) Mahato, S.; Gerling, L. G.; Voz, C.; Alcubilla, R.; Puigdollers, J. High Efficiency ITO-Free Hybrid Solar Cell Using Highly Conductive PEDOT:PSS with Co-Solvent and Surfactant Treatments. *Mater. Lett.* **2017**, *186*, 165−167.
(54) Solazzo, M.; Monaghan, M. G. Structural Crystallisation of Crosslinked 3D PEDOT:PSS Anisotropic Porous Biomaterials to Generate Highly Conductive Platforms for Tissue Engineering Applications. *Biomater. Sci.* **2021**, *9*, 4317−4328.
(55) Tumová, Š.; Malečková, R.; Kubáč, L.; Akrman, J.; Enev, V.; Kalina, L.; Vojtková, E.; Pešková, M.; Víteček, J.; Vala, M.; Weiter, M. Novel Highly Stable Conductive Polymer Composite PEDOT:DBSA for Bioelectronic Applications. *Polym. J.* **2023**, No. 19724.
(56) Shaner, S. W.; Islam, M.; Kristoffersen, M. B.; Azmi, R.; Heissler, S.; Ortiz-Catalan, M.; Korvink, J. G.; Asplund, M. Skin Stimulation and Recording: Moving towards Metal-Free Electrodes. *Biosens. Bioelectron. X* **2022**, *11*, No. 100143.
(57) Shahrim, N. A.; Ahmad, Z.; Wong Azman, A.; Fachmi Buys, Y.; Sarifuddin, N. Mechanisms for Doped PEDOT:PSS Electrical Conductivity Improvement. *Mater. Adv.* **2021**, *2*, 7118−7138.
(58) Hu, Z.; Zhang, J.; Zhu, Y. Effects of Solvent-Treated PEDOT:PSS on Organic Photovoltaic Devices. *Renewable Energy* **2014**, *62*, 100−105.
(59) Li, Z.; Qin, F.; Liu, T.; Ge, R.; Meng, W.; Tong, J.; Xiong, S.; Zhou, Y. Optical Properties and Conductivity of PEDOT:PSS Films Treated by Polyethylenimine Solution for Organic Solar Cells. *Org. Electron.* **2015**, *21*, 144−148.
(60) Huang, J.; Miller, P. F.; Wilson, J. S.; De Mello, A. J.; De Mello, J. C.; Bradley, D. D. C. Investigation of the Effects of Doping and Post-Deposition Treatments on the Conductivity, Morphology, and Work Function of Poly(3,4- Ethylenedioxythiophene)/Poly(Styrene Sulfonate) Films. *Adv. Funct. Mater.* **2005**, *15*, 290−296.
(61) Snaith, H. J.; Kenrick, H.; Chiesa, M.; Friend, R. H. Morphological and Electronic Consequences of Modifications to the Polymer Anode "PEDOT:PSS". *Polymer* **2005**, *46*, 2573−2578.
(62) Liu, P.; Sun, Q.; Zhu, F.; Liu, K.; Jiang, K.; Liu, L.; Li, Q.; Fan, S. Measuring the Work Function of Carbon Nanotubes with Thermionic Method. *Nano Lett.* **2008**, *8*, 647−651.
(63) Su, W. S.; Leung, T. C.; Chan, C. T. Work Function of Single-Walled and Multiwalled Carbon Nanotubes: First-Principles Study. *Phys. Rev. B* **2007**, *76*, 2−9.
(64) Yi, C.; Wilhite, A.; Zhang, L.; Hu, R.; Chuang, S. S. C.; Zheng, J.; Gong, X. Enhanced Thermoelectric Properties of Poly(3,4-Ethylenedioxythiophene):Poly(Styrenesulfonate) by Binary Secondary Dopants. *ACS Appl. Mater. Interfaces* **2015**, *7*, 8984−8989.
(65) Lee, T. W.; Chung, Y. Control of the Surface Composition of a Conducting-Polymer Complex Film to Tune the Work Function. *Adv. Funct. Mater.* **2008**, *18*, 2246−2252.
(66) Castañeda-Uribe, O. A.; Reifenberger, R.; Raman, A.; Avila, A. Depth-Sensitive Subsurface Imaging of Polymer Nanocomposites Using Second Harmonic Kelvin Probe Force Microscopy. *ACS Nano* **2015**, *9*, 2938−2947.
(67) Cassinelli, M.; Park, W. T.; Kim, Y.; Kim, J. H.; Noh, Y. Y.; Caironi, M. Rationalizing the Enhancement of the Thermoelectric Properties of PEDOT:PSS by Secondary Doping. *Appl. Phys. Lett.* **2021**, *119*, No. 033301.
(68) Lee, I.; Kim, G. W.; Yang, M.; Kim, T. Simultaneously Enhancing the Cohesion and Electrical Conductivity of PEDOT:PSS Conductive Polymer Films Using DMSO Additives. *ACS Appl. Mater. Interfaces* **2016**, *8*, 302−310.
(69) Ouyang, J.; Chu, C. W.; Chen, F. C.; Xu, Q.; Yang, Y. High-Conductivity Poly(3,4-Ethylenedioxythiophene):Poly(Styrene Sulfonate) Film and Its Application in Polymer Optoelectronic Devices. *Adv. Funct. Mater.* **2005**, *15*, 203−208.
(70) Lenz, A.; Kariis, H.; Pohl, A.; Persson, P.; Ojamäe, L. The Electronic Structure and Reflectivity of PEDOT:PSS from Density Functional Theory. *Chem. Phys.* **2011**, *384*, 44−51.